Simultaneous Morphological and Flow Imaging Enabled by Megahertz Intravascular Doppler Optical Coherence Tomography

Tianshi Wang, Tom Pfeiffer, Joost Daemen, Frits Mastik, Wolfgang Wieser, A. F. W. van der Steen, Robert Huber, and Gijs van Soest

***Abstract*— We demonstrate three-dimensional intravascular flow imaging compatible with routine clinical image acquisition workflow by means of megahertz (MHz) intravascular Doppler Optical Coherence Tomography (OCT). The OCT system relies on a 1.1 mm diameter motorized imaging catheter and a 1.5 MHz Fourier Domain Mode Locked (FDML) laser. Using a post processing method to compensate the drift of the FDML laser output, we can resolve the Doppler phase shift between two adjoining OCT A-line datasets. By interpretation of the velocity field as measured around the zero phase shift, the flow direction at specific angles can be qualitatively estimated. Imaging experiments were carried out in phantoms, micro channels, and swine coronary artery *in vitro* at a speed of 600 frames/s. The MHz wavelength sweep rate of the OCT system allows us to directly investigate flow velocity of up to 37.5 cm/s while computationally expensive phase-unwrapping has to be applied to measure such high speed using conventional OCT system. The MHz sweep rate also enables a volumetric Doppler imaging even with a fast pullback at 40 mm/s. We present the first simultaneously recorded 3D morphological images and Doppler flow profiles. Flow pattern estimation and three-dimensional structural reconstruction of entire coronary artery are achieved using a single OCT pullback dataset.**

Manuscript received August 7, 2019; revised October 8, 2019; accepted October 15, 2019. Date of publication November 12, 2019; date of current version April 30, 2020. The work of T. Wang and G. van Soest was supported by Nederlandse Organisatie voor Wetenschappelijk (NOW) under Grant Veni-15940 and Grant 104003006. The work of T. Pfeiffer and R. Huber was supported in part by Deutsche Forschungsgemeinschaft (DFG) under Grant DFG·EXC 2167 and in part by H2020 European Research Council (ERC) (ERC CoGFunding. Onderzoek ENCOMOLE-2i, 646669) and the German Federal Ministry of Education and Research (BMBF no. 13GW0227B and BMBF no. 13N14665). *(Corresponding author: Tianshi Wang.)*

T. Wang, J. Daemen, F. Mastik, and G. van Soest are with the Thoraxcenter, Erasmus University Medical Center, 3015 Rotterdam, The Netherlands (e-mail: t.wang.1@erasmusmc.nl).

T. Pfeiffer and R. Huber are with the Institut für Biomedizinische Optik, Universität zu Lübeck, 23562 Lübeck, Germany.

W. Wieser is with Optores GmbH, 80339 München, Germany.

A. F. W. van der Steen is with the Thoraxcenter, Erasmus University Medical Center, 3015 Rotterdam, The Netherlands, with the Shenzhen Institutes of Advanced Technology, Chinese Academy of Sciences, Shenzhen 518055, China, and also with the Department of Imaging science and Technology, Delft University of Technology, 2600 Delft, The Netherlands.

This article has supplementary downloadable material available at http://ieeexplore.ieee.org, provided by the author.

Color versions of one or more of the figures in this article are available online at http://ieeexplore.ieee.org.

Digital Object Identifier 10.1109/TMI.2019.2948258

***Index Terms*— Endoscopy, heart, image acquisition, optical imaging/OCT/DOT, vessels.**

I. Introduction

CORONARY artery disease is associated with the buildup of plaques in the artery wall, narrowing the artery lumen and decreasing the blood flow [1]–[4]. In the assessment of coronary artery disease, both flow and morphological structure are important parameters: the flow measurement characterizes the impaired supply capacity of the artery, while structural information assists in characterization of atherosclerotic plaque and may guide positioning of the stent [5]–[8]. Flow disturbances associated with the stenosis are also hypothesized to influence plaque development [8]. Visualizing the flow pattern and the morphology of the entire coronary artery may provide new insights into functional assessment of coronary artery lesions and enhance our understanding of the progression of atherosclerotic plaques. Previous studies have demonstrated that Magnetic Resonance Imaging and Doppler Ultrasound imaging can visualize carotid flow, as well as morphology, thus enabling early detection of carotid stenosis and its effects on hemodynamics [9], [10]. However, these techniques cannot fully capture the microscopic features of diseased coronary arteries, nor characterize their highly dynamic blood flow patterns in a lumen of only a few millimeters. A fast imaging technique that can simultaneously visualize the flow and morphology with high resolution is highly desired for research, diagnosis and treatment guidance of coronary artery disease.

Intravascular Optical Coherence Tomography (IV-OCT) is a valuable imaging tool for guidance of coronary interventions, capturing morphological details of the artery wall with micrometer resolution and high frame rate [6], [11]. IV-OCT uses a long catheter to deliver light from a wavelength-swept laser inside the artery, illuminating the wall and collecting the back-reflected light through a side-looking reflector. The back-reflected light from the sample arm (comprising the catheter) interferes with the back-reflected light from the reference arm in an interferometer, generating interferogram fringes as a function of wavenumber. The interferogram fringes is Fourier transformed from the wavenumber domain into a complex vector in the spatial domain where the absolute signal contains the morphological information and the phase signal may be processed to extract a Doppler-based measurement of flow in the sample. As a technical extension of OCT, Doppler OCT

enables visualization of vasculature and measurement of blood flow [12]–[14]. Doppler OCT extracts the velocity v of each OCT sample point (at transverse location x and depth z) by measuring the Doppler phase shift $\Delta\varphi$ following,

$$v\,(x,z)\,Cos(\theta) = \frac{\lambda}{4n\pi T}\Delta\varphi\,(x,z) \tag{1}$$

where n is the refractive index of the sample, T is the time delay between two phase measurements. It can be seen that in Doppler OCT, the phase shift is directly related to the velocity projection along the OCT beam that can further be converted to the absolute flow velocity when knowing the Doppler angle θ, e.g. the angle between the direction of the flow velocity and the OCT beam. Although Doppler OCT is a powerful technique, its application is still restricted by two fundamental factors: imaging speed and phase wrapping [12], [13]. First, the phase shift measurements require highly spatially overlapping sample points, thus limiting the beam-scanning speed and thereby the imaging speed. Second, because the measurement of the phase shift is confined to $-\pi$ to π, the shortest time delay T, that depends on the speed of the OCT laser source, decides the maximum measurable velocity [15]. Phase wrapping occurs when the velocity exceeds that maximum. Several techniques such as (computationally expensive) phase unwrapping and split spectrum processing have been developed to address these problems [16], [17]. In particular, Sun et al. demonstrated the first phase-resolved intravascular Doppler OCT by resolving the phase shift between pairs of adjoining A-lines using a 50 kHz OCT system that offers a shortest time delay of 20 μs [15]. Adequate spatial overlap was achieved by increasing the A-line density in each OCT image. However, this method sacrifices the frame rate and the possibility to perform pullback scans. Inevitably, phase-wrapping still occurs because the velocity of coronary blood flow is approximately 15-90 cm/s [18], which is higher than the direct maximum measurable speed. To solve these two problems, we propose to use megahertz (MHz) OCT to resolve the phase shift between adjoining A-lines. The A-line density can be significantly increased while maintaining a high frame rate and a high-speed pullback. On the other hand, the MHz sweep rate decreases the shortest time delay T to less than a microsecond, and the maximum measurable velocity is proportionally increased by 30 times, thus allowing a Doppler OCT measurement of high velocity without requiring a phase-unwrapping.

The Fourier Domain Mode Locked (FDML) laser, used here as an OCT light source, relies on laser mode-locking technology to create a wavelength-swept light output [19]. The output from the main laser cavity is considered to be the master waveform. A buffer stage with appropriate optical delays further converts each master sweep of the laser cavity into a cluster of sweeps that consists of the master sweep itself and several copies. Using this design, a sweep rate greater than a MHz can be achieved based on a master sweep rate of several hundred kilohertz (kHz). Since the first demonstration of OCT imaging using an FDML laser, efforts have been made to advance the development of the instrument, with the aim of increasing not only the wavelength sweep rate but also the stability and operability [19]–[21]. In recent years, the MHz FDML laser has shown its power in Doppler OCT imaging for elastography, measuring rapid tissue motion that previously could not be captured with a low-speed OCT system [22]–[24]. The buffer stage increases the sweep rate but also introduces drifts in time between identical sweep copies. These drifts only depend on the different optical path lengths in the buffer stage and are usually slowly varying mainly due to temperature fluctuations in the fiber. These time drift variations appear as sample offsets of the interferogram fringes in data acquisition, leading to a degraded stability in the phase. Song et al. proposed a strategy to process the phase shift, which considered each cluster output as one group and compared the phase signal between two subsequent master sweeps or two corresponding buffered sweeps [25]. Though this method depresses the phase noise by avoiding the sampling offsets, it stretches the time delay between two phase measurements by a factor of 4, and so restricts the maximum measurable speed. In this study, we measure the variable time drifts by comparing the interferogram fringes of a calibration mirror before imaging and apply compensation in the wavenumber domain during the post-processing. Such method enables accurate phase difference measurements between two adjoining A-lines that corresponds to two adjoining outputs of the FDML laser.

Conventional IV-OCT acquires images using an intravascular catheter that has a rotatable fiber probe. During image acquisition, a proximal motor retracts the fiber probe in the catheter at a preset speed to acquire a volumetric dataset of the entire vessel wall. Recently, a novel motorized catheter has been demonstrated, achieving a higher distal beam-scan speed than can be achieved with the conventional proximate scanning catheters [26], [27]. Super-fast intravascular OCT imaging free of cardiac motion was demonstrated previously by combining a 2.8 MHz FDML laser with a 5600 rotations/s motorized catheter [27], [28]. In this study, we will demonstrate MHz intravascular Doppler OCT using a 1.5 MHz FDML laser modified for phase-sensitive measurement and a newly-developed motorized catheter that has a short rigid length and a large beam angle defined as the angle between the beam and the catheter axis. We demonstrate three-dimensional intravascular flow imaging by capitalizing on the sub-microsecond delays between adjoining A-lines. Computationally expensive phase-unwrapping was avoided and the variable sampling offset, resulting from drifts in the laser buffer stage was corrected. We also show how different cross-sections through the volumetric Doppler dataset allow us to estimate the flow pattern in the entire artery.

II. Methods

A. MHz OCT System and FDML Laser

The OCT system was built based on a 1.5 MHz FDML laser with dispersion compensation. In the FDML laser, the light from a broadband gain media is spectrally filtered by a tunable narrowband optical bandpass filter that only transmits the longitudinal modes with the frequencies within the spectral filter window of the bandpass filter. The tunable optical bandpass filter is periodically driven with a period that is synchronized to the round-trip of the cavity. In such way, the light transmits back to the bandpass filter at a time when the filter is turned

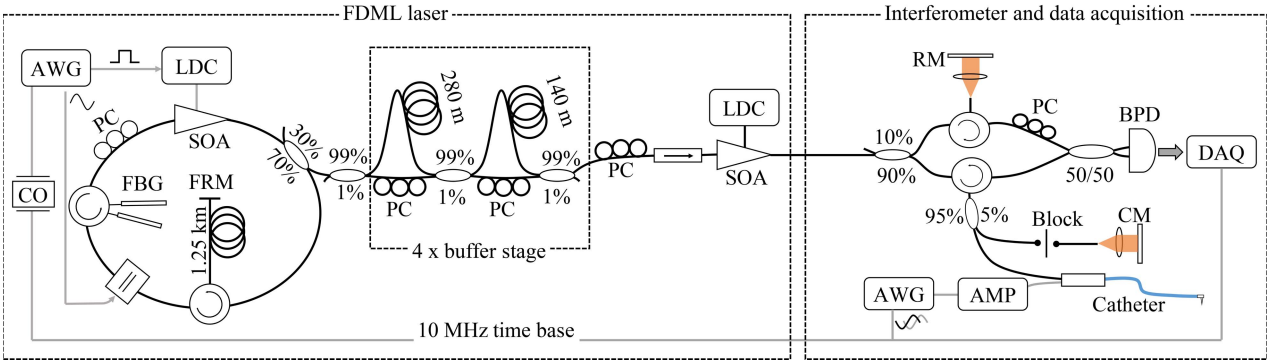

Fig. 1. Schematic diagram of the Megahertz intravascular Doppler OCT system. AWG: arbitrary waveform generator, AMP: current amplifier, BPD: balanced photon detector, CM: calibration mirror, CO: crystal oscillator, DAQ: data acquisition board, FBG: fiber Bragg gating, FFP-TP: Fabry-Pérot tunable filter, FRM: Faraday rotation mirror, LDC: laser diode controller, PC: polarization controller, RM: reference mirror, and SOA: semiconductor optical amplifier.

to the same spectral position again. Therefore, the light does not have to build up repeatedly and a high-power wavelength sweep output is generated.

The schematic diagram of the FDML laser and the entire system is shown in Fig. 1. The FDML laser was built in a Sigma-Ring configuration, the cavity consists of a semiconductor optical amplifier (SOA), a fiber Fabry-Pérot tunable filter (FFP-TF), polarization controllers (PC) and a fiber delay line attached between an optical circulator and a Faraday rotation mirror (FRM). To reduce the dispersion in the cavity, two chirped fiber Bragg gratings (FBG) were used to correct both normal and anomalous dispersion around 1310 nm. The laser cavity runs at a master round-trip frequency of 389 kHz that is controlled by an arbitrary waveform generator (AWG). In order to achieve a 1.5 MHz sweep rate, 4 $\times$ buffer stage was used to convert each master wavelength sweep into a cluster output that consists of one master sweep and 3 delayed copies. The wavelength sweep output has a center wavelength of 1316 nm, a sweep range of 108 nm and an output power of 20 mW on the sample.

Based on the FDML laser, an OCT system was built. The ratio of the sample arm power to the reference arm power was 9:1. In the sample arm, the calibration mirror utilized 5% of the power and the rest of the power was coupled into the imaging catheter. A 1.6 GHz balanced photo receiver (ThorLabs, NJ) and a 4 GS/s 8-bit data acquisition board (Gage, NY) were used to record the interferogram fringes. To improve the accuracy of data acquisition and the phase measurement, a 10 MHz time base was generated by a crystal oscillator, synchronizing the bandpass filter of the FDML laser, the driving signal of the catheter, and the data acquisition card. The OCT system finally achieves an axial resolution of 11.9 μm, a transverse resolution of 22.9 μm (beam waist), a sensitivity of 102 dB with 20 mW output power, and a 6 dB sensitivity roll-off imaging depth of 4.0 mm in air.[1] Interference fringes of a calibration mirror were acquired automatically before each imaging experiment for background noise subtraction and wavenumber linearity calibration. In addition, the fringes of the calibration mirror were also used to compensate the sampling offsets induced by the laser buffer stage and improve the phase measurement.

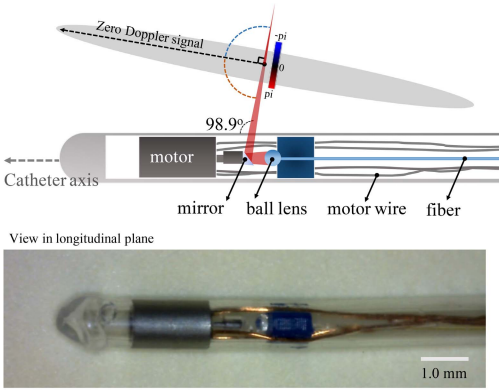

Fig. 2. Schematic diagram and photograph of the motorized catheter, shown in longitudinal plane.

B. Motorized Catheter With Large Beam Angle

In this study, a motorized catheter was built, whose schematic diagram and photograph are shown in Fig. 2. The gradient refractive index lens used in our previous studies was replaced by a 2.0 mm diameter ball lens probe, which improves the flexibility of the catheter tip by reducing the rigid length from 5.3 mm to 4.2 mm. The laser beam forms a Gaussian beam waist of 22.9 μm at 1.4 mm distance (in air) from the catheter sheath. The final dimension of the catheter is 1.1 mm outer diameter and 1.6 meter length. The transparent outer sheath was made by biocompatible polyether block amide. The velocity characterization of the micromotor and the beam characterization of the catheter can be found in the supplementary material.[2]

The measurement of the Doppler phase shift is sensitive to the angle between the OCT beam and the direction of flow. According to (1), a measured zero phase shift indicates that the projection of the three-dimensional (3D) flow vector that is parallel to the OCT beam equals to zero, even when the velocity itself is not zero. Considering Fig. 2 as a 2D longitudinal imaging plane, the projection of the flow vector onto this plane (black dashed arrow in Fig. 2) will be perpendicular to the OCT beam as well and form a specific angle to the OCT catheter. By detecting the zero phase shift and interpreting the zero-crossing features, we can qualitatively

[1]Supplementary Note 1

[2]Supplementary Note 2 and 3

estimate the pattern of the flow projection in the longitudinal plane. For this reason, we increased the beam angle of the catheter to 102° as measured geometrically in air (98.9° in intralipid), when the commercial catheter normally has a beam angle of 80°. The large beam angle allowed us to qualitatively estimate the flow pattern near the black dashed arrow in Fig.2, which forms an angle of 8.9°(in intralipid) to the catheter within the longitudinal imaging plane.

The micromotor used in the catheter is a synchronous two-phase 4-pole micromotor that consists of a stator coil and a permanent magnet rotor.[3] By sending two sinusoidal current waveforms to the coil with $\pi/2$ phase difference, a rotating magnetic field can be created, which further rotates the permanent magnet rotor. The rotating speed of the motor is always synchronized to the frequency of the sinusoidal current waves. The effective current value required for 600 revolutions/s was 350 mA for each channel, which corresponds to a frame rate of 600 frames/s.

C. Experimental Set Up

To validate the Doppler OCT imaging, we prepared a 10% weight-solution Poly Vinyl Alcohol (PVA) hydrogel phantom with 3 freeze-thaw cycles [29]. The lumen of the phantom was formed into the shape of a shield using a custom mold. Intralipid (0.5% v/v) was used as the Doppler imaging contrast. A homemade infusion pump was built by attaching a 30 ml syringe (BD, NJ) to a linear motor stage (Areotech, PA). A programmable infusion rate can be achieved by controlling the speed of the motor stage. For catheter-based Doppler imaging experiments, an 8 French guiding catheter was used to guide both the imaging catheter and the intralipid into the phantom or the swine coronary arteries.

D. Doppler Signal Processing

To compensate the sampling offsets induced by the laser buffer stage, interferogram fringes of calibration mirror was acquired before each imaging. The sampling offsets were then found by calculating the cross-correlation of the fringes of each buffered A-line and the fringes of the master A-line. As the first step of post-image processing, each buffered A-line dataset was shifted according to the measured sampling offset. Thereafter, the background noise was subtracted and the interferogram was resampled to achieve a linear distribution in the wavenumber space. Then, a Fast Fourier Transform (FFT) was performed to convert the interferogram fringes in the wavenumber domain to a complex dataset in spatial domain. The absolute signal of the complex data was used to reconstruct conventional morphological OCT images. The phase shift $\Delta\varphi$ of each sample point was extracted between two adjoining A-lines from the complex OCT data I following

$$\Delta\varphi\,(j,i) = tan^{-1}\left\{\frac{Im[I\,(j,i)\,I^{*}\,(j,i+1)]}{Re[I\,(j,i)\,I^{*}\,(j,i+1)]}\right\} \qquad (2)$$

where j is the index of the sample point and i is the index of A-line. As the final step, the phase shift was converted into velocity following (1) to create Doppler images.

[3]Supplementary Note 2

The distortion of the small mirror in the catheter induces an offset error to the phase-shift of entire A-line of the Doppler image. In the Doppler image, this error can be observed as offset artifacts on the stable samples and the catheter tube. We compensated for this error by subtracting the phase shift of the catheter sheath in the entire Doppler A-line, similar to what had been done in a previous study conducted by Sun et al. [15]. The analysis of the distortion-induced phase error and compensation is described in the supplement material.[4]

III. Results

A. Sampling-Offset Analysis and Compensation

The intensity returned from the mirror used in the calibration measurements is shown in Fig. 3(a). Fig. 3(b) shows four adjoining pieces of interferogram fringes of the mirror, corresponding to one cluster output of the FDML laser. Each fringe trace consists of 2398 sample points. Due to the sampling offsets, the fringes are not aligned and the drift between the fringes can be seen in Fig. 3(c). By calculating the cross-correlation of the fringes after upsampling by 10 times, sampling offsets for the three buffered A-lines were found to be −20.7, −24.5, and −31.5 sample points relative to the master A-line. Based on the measured offsets, the recorded fringes of each buffered A-line were shifted back accordingly. Fig. 3(d) shows the fringes of the 4 A-lines matched after the compensation. To validate the phase-shift measurement, an M-Mode image (no beam scanning) of a glass coverslip was acquired at 2.0 mm depth and the Doppler phase noise was analyzed before and after the compensation. Fig. 3(e) shows the phase shift between two adjoining A-lines measured on the coverslip surface. Large phase noise associated with cyclical fluctuations in groups of four sample points can be seen, which is due to the cluster output of the FDML laser and the sampling offsets induced by the buffer stage. Fig. 3(f) shows the phase shift after compensating for the sampling offsets and it can be seen that the cyclical fluctuations were significantly depressed. Since the phase shift of the stable coverslip surface is expected to be zero, root-mean-square error (RMSE) of the phase shift was calculated for evaluation, which was reduced from 1.60 rad to 0.01 rad using our compensation method.

B. Doppler Imaging Validation in Phantom

The PVA phantom was flushed with intralipid at a rate of 3 ml/s. The OCT system was operated at 600 frames/s so the A-line density is 2592 A-lines per frame, which is much higher than the conventional density of around 500 A-lines per frame. Such high A-line density ensures a beam overlap of >86% when processing the phase shift between two adjoining A-lines. Fig. 4(a) shows the intensity image that was reconstructed using the absolute value of the complex OCT dataset. Structure features of the shield-shape lumen of the PVA phantom and the speckle of the flowing intralipid can be clearly seen in the image. Four shadow areas can also be seen, which were caused by the motor wires. Fig. 4(b) shows the

[4]Supplementary Note 4

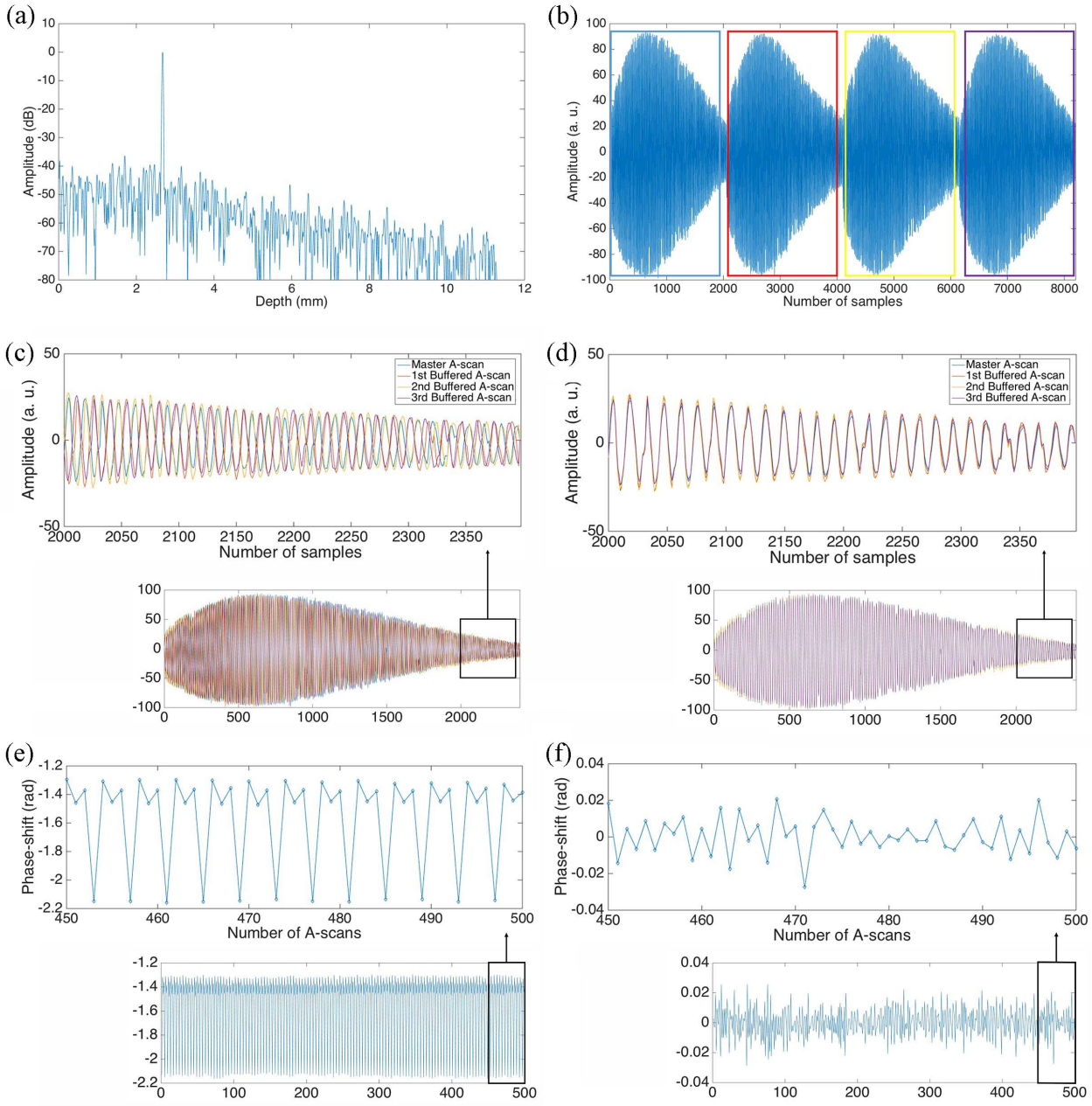

Fig. 3. Schematic diagram of sampling-offset compensation. (a) Plot of one intensity A-line showing the calibration mirror put at 2.5 mm distance. (b) Interferogram fringes of the mirror corresponding to 4 A-lines containing one master A-line (blue) and three buffered A-lines (red, yellow, and purple). (c) Fringes of 4 A-lines overlaid to show the sampling-offset problem. (d) Fringes shifted according to the measured sampling offsets. (e) Phase-shift of two adjoining A-lines measured on the surface of a coverslip without sampling-offset compensation. (f) Phase-shift of two adjoining A-lines measured on the surface of the coverslip after the sampling-offset compensation.

Doppler image that was reconstructed by calculating the phase shift between two adjoining A-lines. Due to the sampling offsets, Doppler information is completely washed out by the phase noise. In contrast, after applying the sampling-offset compensation, the Doppler information appears in Fig. 4(c), and the flowing intralipid and the stable PVA phantom are clearly visible and easily distinguished. It is worth mentioning that the dynamic contrast of the Doppler image is related to the velocity, while the contrast of OCT image depends on the optical backscattering and reflection of the sample. The marked area in Fig. 4(c) shows the distortion-induced artifact on the phantom. To reduce the artifact, the measured phase shift of each A-line was subtracted by the phase shift of the catheter sheath. Using this method, the distortion artifact is effectively depressed, as shown in Fig. 4(d). The RMSE of the phase shift of the stable phantom lumen was reduced from 0.19 rad to 0.08 rad.[5]

C. Flow Measurement Validation in Microchannel

The 1.5 MHz sweep rate of the FDML laser allows us to resolve the phase shift with a shortest time delay of 0.67 μs (between two adjoining A-lines). According to (1), the velocity

[5]Supplementary Note 4

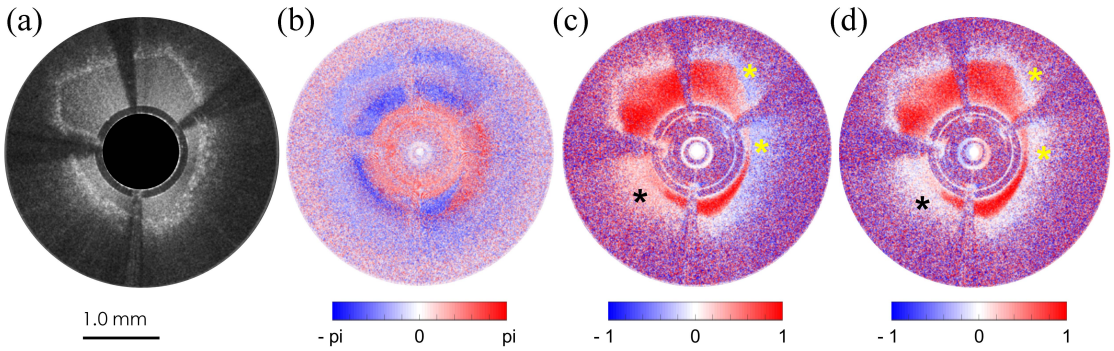

Fig. 4. Doppler OCT imaging of phantom and intralipid. (a) Intensity image of PVA phantom and intralipid. (b) Phase-shift between two adjoining A-lines without sampling-offset compensation. (c) Phase-shift between two adjoining A-lines after sampling-offset compensation. (d) Phase-shift extracted between two adjoining A-lines after sampling-offset compensation and distortion error correction. The color bar corresponds to the phase-shift. Star marks indicate the distortion-induced artifacts before and after the compensation.

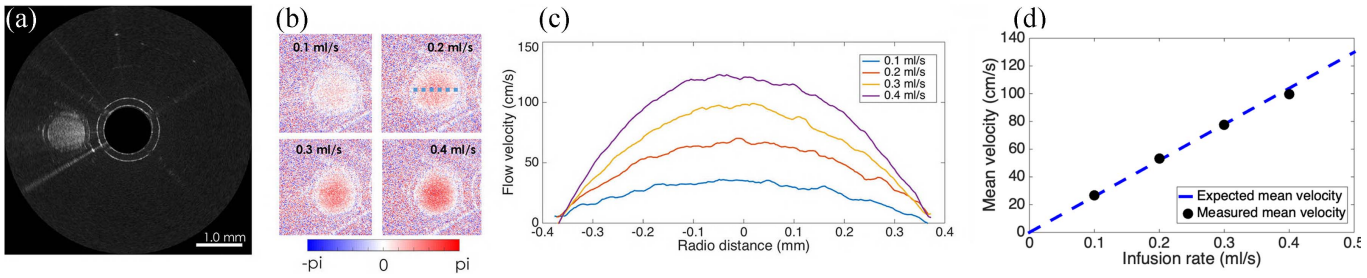

Fig. 5. Doppler imaging and velocity measurement of intralipid flowing in a 0.7 mm diameter microtube at different infusion rates. (a) intensity image of the intralipid and microtube, (b) Doppler images acquired at different infusion rates. (c) measured speed profile of the blue dashed line in b. (d) Comparison between measured and expected velocities. The measured speed projection was converted into absolute flow, taking into account the 112° beam angle. Each speed profile was averaged over 10 frames to create a statistically stable profile.

projection along OCT beam can be directly measured within a large range of approximately −37.5 to 37.5 cm/s without any phase unwrapping. To validate the velocity measurement, the intralipid was injected into a 0.7 mm diameter microtube that was put in parallel with the catheter. Doppler images acquired at different infusion rates were analyzed. Since the tube was in parallel with the catheter, the measured velocity projection was converted into the absolute flow velocity, accounting for the Doppler angle. The measurable range along the tube then is approximately −242 to 242 cm/s. Fig. 5(a) shows the intensity image of the microtube, the flowing intralipid, and the motorized catheter. Fig. 5(b) shows the Doppler images acquired at different infusion rates. Clearly, a higher infusion rate leads to a larger phase shift. Speed profiles along the dashed line in Fig. 5(b) were produced by averaging over 10 frames (16 ms). The speed profiles are plotted in Fig. 5(c). The mean value of each speed profile was further calculated and compared with the expected velocity. The results in Fig. 5(d) show that the measured velocities agree well with the theoretical calculation.

D. Dynamic Flow Imaging in a Coronary Artery

Dynamic flow in a swine coronary artery was induced by changing the infusion rate from proximal end dynamically. A homemade pump was programmed to decrease the rate from 3 to 0 ml/s and then increase to 1 ml/s. The entire process lasted for one second and the Doppler images were acquired near a side branch at the distal end. The imaging speed was set to 600 frames/s. Doppler images of the flow pattern and the structural images of the arterial wall were reconstructed using the single dataset. To better distinguish the Doppler information from the grayscale morphological OCT information, the color scale of the Doppler image was modified. Four Doppler images acquired at different infusion rates were segmented manually and overlaid on top of the structural images, as shown in Fig. 6. The imaging results show that a large infusion rate leads not only to a high velocity projection along the OCT beam but also to a large lumen size of the artery due to the elevated pressure. Doppler and OCT images of the entire dynamic process were further converted into a video,[6] showing the flow pattern changing and artery wall motion side by side.

E. Flow Pattern Imaging in Longitudinal Imaging Plane

The MHz intravascular Doppler OCT system resolves the phase shift with a time delay of 0.67 μs. Such a short time scale allows us to further expand the intravascular Doppler imaging from 2D imaging at a fixed location to 3D Doppler imaging using a pullback scan. A 40 mm/s pullback speed can potentially induce a velocity of 6.2 mm/s along the OCT beam, which leads to an error of −0.06 rad to the phase-shift measurement. This tiny phase-shift error could be subtracted

[6]Media 1: Doppler-OCT imaging of dynamic flow

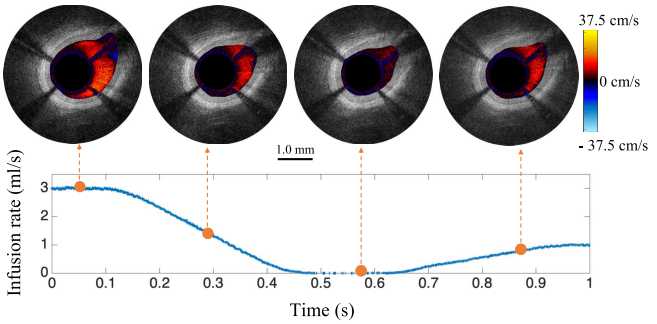

Fig. 6. Overlaid Doppler OCT images acquired at different infusion rates. The color bar indicates the measured velocity projection along the OCT beam.

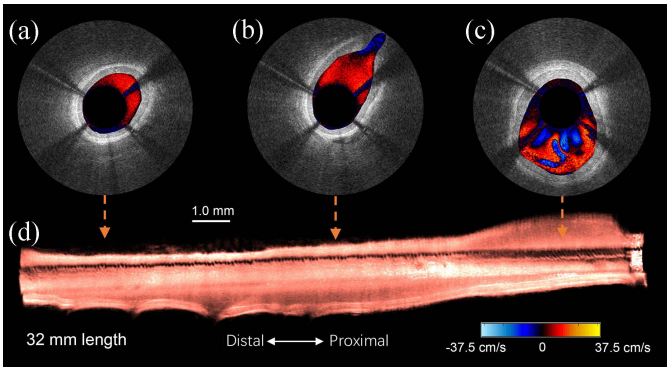

Fig. 7. Doppler images overlaid with structural images acquired at different locations of the coronary artery. (a) overlaid Doppler OCT images acquired at distal end. (b) overlaid Doppler-OCT image acquired near a sidebranch. (c) overlaid Doppler-OCT image acquired at proximal end. (d) 3D reconstruction of the coronary using the OCT structural images. The overlaid Doppler-OCT images and the 3D reconstruction were reconstructed using single dataset acquired at 40 mm/s pullback speed and 600 frames/s imaging speed. The color bar indicates the velocity measured along the OCT beam.

in the measured phase shift in post processing. On the other hand, a pullback also induces a beam mismatch of 27 nm between two adjoining A-lines. However, this small mismatch is negligible compared to the beam radius of >22.9 μm along the OCT beam.

The first 3D intravascular Doppler OCT imaging was conducted in a swine coronary artery *in vitro* while running the system at 600 frames/s and 40 mm/s pullback (frame pitch of 67 μm). The infusion rate was set to 3 ml/s. Using the single pullback dataset, morphological OCT images and Doppler images were reconstructed and converted into a video.[7] In Fig. 7(d), a 3D reconstruction was made based on the intensity signal, which shows the morphological structure of the whole artery. Three Doppler–OCT overlaid images acquired at different locations are shown in Fig. 7 (a-c). At the distal end of the artery, a more homogenous flow pattern can be observed. However, negative Doppler velocity can be seen when the image was acquired near a side branch as shown in Fig. 7(b). At the proximal end, the Doppler image shows even more complicated patterns, as shown in Fig. 7(c). This is because the small lumen size at the distal end restricts the flow direction to be more in parallel with the catheter. Therefore, the angle between the flow direction and the OCT beam is less than 90° and the phase shift was measured to be positive. However, at the proximal end or near a side branch, the flow pattern is complex and the angle between the flow direction and the OCT beam could be larger than 90°, leading to a negative Doppler phase shift. Specifically, zero-crossing of the phase shift (e.g. red to black to blue color change) can be seen in Fig. 7(b), indicating that the intralipid flowed into the side branch and the angle between the velocity and the OCT beam changed from $<90°$ to $>90°$ near this area. Beyond the cross-sectional Doppler image, flow direction can further be estimated in the longitudinal imaging plane, which gives a better view of the flow pattern in the entire coronary artery. Fig. 8 shows the overlaid longitudinal Doppler OCT image. The Doppler signal was also obtained using pairs of adjoining A-lines within one cross-sectional frame. A zero phase shift indicates that the direction of the velocity projection is perpendicular to the OCT beam, forming an 8.9° angle to the catheter as shown in Fig. 2. This qualitative flow direction estimation was marked by yellow arrows in Fig. 8. The zoomed area at the top left shows zero-crossing features e.g. red-black-blue color changing from proximal to distal, which indicates that the angle between the flow direction and catheter changes from $<8.9°$ to $>8.9°$. The estimated direction changes are marked by white arrows in the longitudinal image. Similarly, the zoomed area at the top right indicates that the flow angle changes from $<8.9°$ to $>8.9°$ then back to $<8.9°$ to the catheter. The flow estimation of the top part of the Fig. 8 shows that the intralipid tends to flow along the geometry of the artery wall, which is consistent with hemodynamic models [30], [31]. Using the same methods, the flow direction change induced by the three bifurcations (bottom part of the Fig. 8) were also estimated. A video consisting of both the longitudinal intensity image and the Doppler image was produced,[8] allowing us to inspect the flow pattern and the structure of the entire artery at the same time. It is worth noting that a zero flow velocity or a flow direction with 98.9° to the catheter can both appear as a zero phase shift. However, in qualitative interpretation of the flow patterns, this confounding factor can be excluded since flow is applied from the proximal to distal end in the coronary artery, so nonzero flow velocity can be assumed. Similar to most 2D Doppler imaging techniques, our identification of flow patterns is only applicable in the longitudinal image plane, and the direction estimation is applicable to the velocity projection on this plane, which is not the absolute flow direction in 3D space.

IV. Discussion

In this study, we demonstrate MHz intravascular Doppler OCT that relies upon a motorized catheter with a large beam angle and a phase-sensitive FDML OCT system. The flow rate in the coronary artery can be over 90 cm/s. To capture a such high velocity, conventional IV-OCT systems have to apply computationally expensive algorithms and sacrifice the imaging speed and pullback. As a new approach, the MHz speed of our prototype allows us to directly measure the velocity projection along the OCT beam within a range of 37.5 cm/s,

[7]Media 2: Doppler-OCT pullback record

[8]Media 3: Longitudinal view of Doppler-OCT pullback record

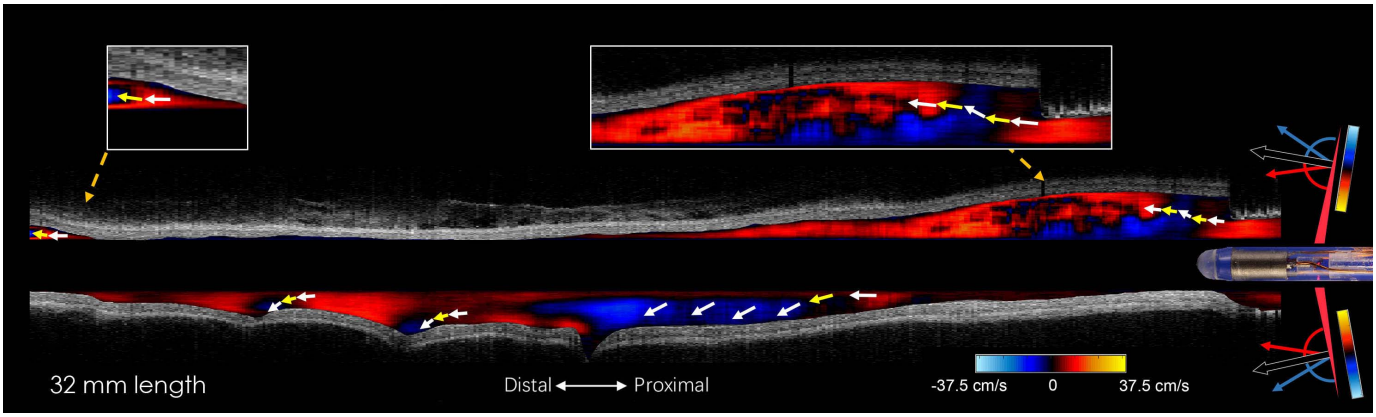

Fig. 8. Overlaid longitudinal Doppler OCT image of the entire coronary artery. Yellow arrows indicate that the direction of the velocity projection on the longitudinal image plane is perpendicular to the OCT beam. White arrows are the estimation of the direction of the velocity projection near the zero-crossing (yellow arrows) based on the crossing pattern. The schematic diagram of the catheter on the right part demonstrates how the Doppler image color scale indicates the measured velocity along the OCT beam.

which corresponds to a velocity of approximately 242 cm/s parallel to the catheter. Furthermore, 3D Doppler OCT dataset containing morphological and Doppler information of the entire coronary can be acquired in single pullback, and be fully processed within minutes after data acquisition.

A flow direction that is perpendicular to the OCT beam induces a zero phase shift. We observed this near the bifurcations and at the proximal end of the artery. By investigating the zero crossing feature of the phase shift, the flow direction was estimated in the longitudinal imaging plane. In Doppler-based flow imaging, the flow estimation is only sensitive to a specific angle that is decided by the beam angle of the catheter. In the catheter design, we chose a 102° beam angle to estimate the flow direction that forms an 8.9° angle to the catheter; this value is close to the angle between the side branches and the main branch, which makes the flow direction estimation more sensitive to the bifurcations. In the future, a catheter that integrates two OCT optical paths with different beam angles might potentially be developed to provide more information on the flow pattern, similar to dual-beam Doppler OCT imaging [32]. A quantitative absolute flow measurement could potentially be achieved in single measurement by combining the Doppler measurement with the speckle decorrelation technique that is capable of measuring the transverse flow projection in weakly optically scattering fluids [33], [34]. It is worth mentioning that a higher A-line density might be required by the speckle decorrelation algorithm, which could possibly be achieved by decreasing the frame rate of our system to $<$200 frames/s.

To address the fringe drift induced by the buffer stage, we proposed a post-processing method to compensate for the sampling offsets without using additional optical components such as FBGs or k-clock triggering. This method allows us to extract the phase shift with a time delay of arbitrary number of A-lines, making full use of the 1.5 MHz sweep rate. Based on this, not only flow but also fast tissue motion could be monitored continuously with a time resolution of 0.67 μs. This might potentially benefit other OCT techniques, such as optical coherence elastography [35], photo-thermal OCT and thermo-elastic OCT [23], [36]. The sampling offset problem is induced by the long optical fiber of the buffer stage. In principle, when the refractive index of the fiber remains the same, the sampling offsets can be measured for once and used for all imaging experiments afterwards. However, environmental factors, especially temperature fluctuations, may affect the refractive index of the long fibers in the buffer stage, leading to a slowly varying sampling offset. Therefore, in our study, the calibration fringes were recorded before the imaging experiment each time, which only took a couple of seconds. A temperature control of the buffer stage might also be applied, which would help maintain constant sampling offsets over a longer time scale [37]. Besides the buffer stage, many other factors can affect the phase stability of the system, including temperature change of the interferometer, reference-arm fluctuation, spectrum variance of the laser and the sampling jitter of the digitizer [38], [39]. In our study, the phase shift was extracted with a time delay of 0.67 μs. For such a relatively short time scale, the temperature change and the reference-arm fluctuation are negligible. The phase stability is mainly affected by the spectrum variance of the laser and the sub-sample jitter, which result in a final phase stability of 10 mrad (1.0 nm in air) within 2.0 mm imaging depth as a velocity noise of 1.6 mm/s. Such a stability is sufficient for the Doppler imaging for our study. In addition to the phase stability of the system, the phase error induced by the rotation distortion of the catheter mainly affects the Doppler measurement. The 80 mrad error after the distortion compensation can still lead to 0.94 cm/s error to the velocity measurement, which would contribute to the experimental error in the flow validation using the microchannel. A relatively large error of 4.4 cm/s (4.2 % error) was measured when the infusion rate was set to 0.4 ml/s. This might be because a higher infusion rate induced a stronger flow fluctuation that affects the flow direction of the intralipid, thus leading to a lower measured velocity. It is worthwhile to mention that Vakoc et al. also demonstrated a phase correction method using a calibration mirror [40]. However, our correction is directly applied to the original interferogram fringes in the wavenumber domain while the

method proposed by Vakoc et al. subtracts the phase variation in the time domain after FFT.

Physiological assessments of the severity of CAD can be realized by measuring the coronary flow or pressure [5], [7]. The dynamic flow imaging demonstrated here, performed at the distal end of a coronary artery, may potentially be used to provide a Coronary Flow Reserve (CFR) measurement, as the relative ratio of the hyperemic intracoronary flow during an infusion of adenosine over the baseline flow. For clinical practice, Doppler-OCT-based flow measurement combined with another pressure-based measurement may potentially achieve more comprehensive assessments of stenosis, thus leading to better clinical decision making. Coronary microvascular disease (MVD) is a heart disease that is characterized by dysfunction and poor perfusion of small sidebranches, distal microvessels, and capillaries, affecting the delivery of oxygen and nutrients to the myocardium [41]. The diagnosis of MVD has been a challenge since the pressure-based functional tests used for CAD assessment cannot adequately identify MVD. The flow pattern imaging demonstrated in this study can provide flow information near the side branches in the coronary artery tree, which can potentially provide information on microvascular resistance and thus aid diagnosis of MVD. Wall shear stress (WSS) is the frictional force on the artery wall induced by the flowing of blood [8]. Many studies have shown that WSS is playing an essential role in the formation and progression of atherosclerotic plaque. Typically, the WSS profile is created based on computational fluid dynamics (CFD) calculations, which relies on the vessel geometry, but also strongly depends on the assumed, and principally unknown, inflow and outflow conditions. The MHz Doppler OCT demonstrated in this study visualizes the flow pattern and arterial geometry with micrometer scale resolution. As a high-precision flow imaging technique, it may quantify the relevant flow parameters for CFD, but also directly shed light on the interaction between blood flow and arterial abnormalities.

As a limitation, the insertion of the catheter can affect the flow pattern inside the coronary artery because the catheter's cross-sectional area reduces the free lumen. Previous studies have demonstrated that the peak to mean flow ratio in the coronary artery is reduced by approximately 14-24% and the WSS value is also affected [42], [43]. However, by accounting for the catheter size and its location inside the artery lumen, this influence can potentially be compensated [42], [43].

Due to the strong attenuation of the OCT signal in blood, to apply this technique to pre-clinical and clinical applications, we will investigate the clinical safety of using intralipid as intravascular flushing agent and also evaluate other types of imaging contrasts, including diluted blood, microbubbles and nanoparticles [15], [44], [45]. It is also important noting that, besides the motorized catheter used in this study, the MHz OCT system is also compatible with commercial catheters that are in clinical use, although the frame rate will be severely limited by the rotation speed of the rotary junction. Doppler imaging based on commercial catheters will be more readily applicable for future patient studies.

V. Conclusion

We demonstrate MHz intravascular Doppler OCT that can directly measure a velocity projection along OCT beam within a range of 37.5 cm/s without phase wrapping. Morphological and Doppler flow pattern imaging were simultaneously achieved at an imaging speed of 600 frames/s and a pullback speed of 40 mm/s. Using MHz intravascular Doppler OCT, we realize the first *in vitro* 3D intravascular Doppler imaging: visualizing the dynamic flow pattern at fixed location and estimating the flow pattern of the entire coronary artery in longitudinal view. The 3D Doppler information will potentially provide new opportunities for coronary flow studies and diagnosis, such as CFR measurement, MVD diagnosis and WSS profile estimation.

Acknowledgment

The authors acknowledge Geert Springeling for his contribution to the catheter manufacturing and phantom preparation. The authors acknowledge A. López-Marín for his contribution to the characterization of the catheter.

References

[1] A. J. Lusis, "Atherosclerosis," *Nature*, vol. 407, no. 6801, pp. 233–241, Sep. 2000.
[2] E. Falk, "Pathogenesis of atherosclerosis," *J. Amer. College Cardiol.*, vol. 47, no. 8, pp. C7–C12, Apr. 2006.
[3] R. Virmani, F. D. Kolodgie, A. P. Burke, A. Farb, and S. M. Schwartz, "Lessons from sudden coronary death: A comprehensive morphological classification scheme for atherosclerotic lesions," *Arteriosclerosis, Thrombosis, Vascular Biol.*, vol. 20, no. 5, pp. 1262–1275, May 2000.
[4] T. Thim *et al.*, "Wall shear stress and local plaque development in stenosed carotid arteries of hypercholesterolemic minipigs," *J. Cardiovascular Disease Res.*, vol. 3, no. 2, pp. 76–83, Apr./Jun. 2012.
[5] N. H. J. Pijls *et al.*, "Measurement of fractional flow reserve to assess the functional severity of coronary-artery stenoses," *New England J. Med.*, vol. 334, no. 26, pp. 1703–1708, Jun. 1996.
[6] G. J. Tearney *et al.*, "Consensus standards for acquisition, measurement, and reporting of intravascular optical coherence tomography studies: A report from the international working group for intravascular optical coherence tomography standardization and validation," *J. Amer. College Cardiol.*, vol. 59, no. 12, pp. 1058–1072, Mar. 2012.
[7] L. Cortigiani *et al.*, "Coronary flow reserve during dipyridamole stress echocardiography predicts mortality," *JACC, Cardiovascular Imag.*, vol. 5, no. 11, pp. 1079–1085, Nov. 2012.
[8] S. S. Dhawan *et al.*, "Shear stress and plaque development," *Expert Rev. Cardiovascular Therapy*, vol. 8, no. 4, pp. 545–556, Apr. 2010.
[9] M. D. Hope *et al.*, "Clinical evaluation of aortic coarctation with 4D flow MR imaging," *J. Magn. Reson. Imag., Off. J. Int. Soc. Magn. Reson. Med.*, vol. 31, no. 3, pp. 711–718, Mar. 2010.
[10] D. Gaitini and M. Soudack, "Diagnosing carotid stenosis by Doppler sonography: State of the art," *J. Ultrasound Med.*, vol. 24, no. 8, pp. 1127–1136, Aug. 2005.
[11] B. E. Bouma *et al.*, "Evaluation of intracoronary stenting by intravascular optical coherence tomography," *Heart*, vol. 89, no. 3, pp. 317–320, Mar. 2003.
[12] R. A. Leitgeb, R. M. Werkmeister, C. Blatter, and L. Schmetterer, "Doppler optical coherence tomography," *Prog. Retinal Eye Res.*, vol. 41, no. 100, pp. 26–43, 2014.
[13] A. Szkulmowska, M. Szkulmowski, A. Kowalczyk, and M. Wojtkowski, "Phase-resolved Doppler optical coherence tomography—Limitations and improvements," *Opt. Lett.*, vol. 33, no. 13, pp. 1425–1427, Jul. 2008.
[14] S. Makita, T. Fabritius, and Y. Yasuno, "Quantitative retinal-blood flow measurement with three-dimensional vessel geometry determination using ultrahigh-resolution Doppler optical coherence angiography," *Opt. Lett.*, vol. 33, no. 8, pp. 836–838, Apr. 2008.
[15] C. Sun *et al.*, "*In vivo* feasibility of endovascular Doppler optical coherence tomography," *Biomed. Opt. Express*, vol. 3, no. 10, pp. 2600–2610, Oct. 2012.

[16] B. Vuong *et al.*, "High speed, wide velocity dynamic range Doppler optical coherence tomography (Part IV): Split spectrum processing in rotary catheter probes," *Opt. Express*, vol. 22, no. 7, pp. 7399–7415, Apr. 2014.

[17] H. C. Hendargo, M. Zhao, N. Shepherd, and J. A. Izatt, "Synthetic wavelength based phase unwrapping in spectral domain optical coherence tomography," *Opt. Express*, vol. 17, no. 7, pp. 5039–5051, Mar. 2009.

[18] E. O. Ofili *et al.*, "Analysis of coronary blood flow velocity dynamics in angiographicaily normal and stenosed arteries before and after endolumen enlargement by angioplasty," *J. Amer. College Cardiol.*, vol. 21, no. 2, pp. 308–316, Feb. 1993.

[19] R. Huber, M. Wojtkowski, and J. G. Fujimoto, "Fourier domain mode locking (FDML): A new laser operating regime and applications for optical coherence tomography," *Opt. Express*, vol. 14, no. 8, pp. 3225–3237, Apr. 2006.

[20] W. Wieser, B. R. Biedermann, T. Klein, C. M. Eigenwillig, and R. Huber, "Multi-megahertz OCT: High quality 3D imaging at 20 million A-scans and 4.5 GVoxels per second," *Opt. Express*, vol. 18, no. 14, pp. 14685–14704, Jul. 2010.

[21] W. Wieser, T. Klein, W. Draxinger, and R. Huber, "Fully automated 1.5 MHz FDML laser with more than 100 mW output power at 1310 nm," *Proc. SPIE*, vol. 9541, Jul. 2015, Art. no. 954116.

[22] M. Singh *et al.*, "Phase-sensitive optical coherence elastography at 1.5 million A-lines per second," *Opt. Lett.*, vol. 40, no. 11, pp. 2588–2591, Jun. 2015.

[23] T. Wang *et al.*, "Thermo-elastic optical coherence tomography," *Opt. Lett.*, vol. 42, no. 17, pp. 3466–3469, Sep. 2017.

[24] D. C. Adler, S.-W. Huang, R. Huber, and J. G. Fujimoto, "Photothermal detection of gold nanoparticles using phase-sensitive optical coherence tomography," *Opt. Express*, vol. 16, no. 7, pp. 4376–4393, Mar. 2008.

[25] S. Song *et al.*, "Strategies to improve phase-stability of ultrafast swept source optical coherence tomography for single shot imaging of transient mechanical waves at 16 kHz frame rate," *Appl. Phys. Lett.*, vol. 108, no. 19, May 2016, Art. no. 191104.

[26] T. Wang *et al.*, "Intravascular optical coherence tomography imaging at 3200 frames per second," *Opt. Lett.*, vol. 38, no. 10, pp. 1715–1717, May 2013.

[27] T. Wang *et al.*, "Heartbeat OCT: *In vivo* intravascular megahertz-optical coherence tomography," *Biomed. Opt. Express*, vol. 6, no. 12, pp. 5021–5032, Dec. 2015.

[28] T. Wang *et al.*, "Heartbeat OCT and motion-free 3D *in vivo* coronary artery microscopy," *JACC, Cardiovascular Imag.*, vol. 9, no. 5, pp. 622–623, May 2016.

[29] A. Kharine *et al.*, "Poly(vinyl alcohol) gels for use as tissue phantoms in photoacoustic mammography," *Phys. Med. Biol.*, vol. 48, no. 3, p. 357, Jan. 2003.

[30] H. Ha *et al.*, "The influence of the aortic valve angle on the hemodynamic features of the thoracic aorta," *Sci. Rep.*, vol. 6, Aug. 2016, Art. no. 32316.

[31] C. Peng *et al.*, "The impact of the geometric characteristics on the hemodynamics in the stenotic coronary artery," *PLoS ONE*, vol. 11, no. 6, Jun. 2016, Art. no. e0157490.

[32] C. Dai, X. Liu, H. F. Zhang, C. A. Puliafito, and S. Jiao, "Absolute retinal blood flow measurement with a dual-beam Doppler optical coherence tomography," *Investigative Ophthalmol. Vis. Sci.*, vol. 54, no. 13, pp. 7998–8003, Dec. 2013.

[33] N. Uribe-Patarroyo, M. Villiger, and B. E. Bouma, "Quantitative technique for robust and noise-tolerant speed measurements based on speckle decorrelation in optical coherence tomography," *Opt. Express*, vol. 22, no. 20, pp. 24411–24429, Oct. 2014.

[34] X. Liu, Y. Huang, J. C. Ramella-Roman, S. A. Mathews, and J. U. Kang, "Quantitative transverse flow measurement using optical coherence tomography speckle decorrelation analysis," *Opt. Lett.*, vol. 38, no. 5, pp. 805–807, Mar. 2013.

[35] K. V. Larin and D. D. Sampson, "Optical coherence elastography—OCT at work in tissue biomechanics [invited]," *Biomed. Opt. Express*, vol. 8, no. 2, pp. 1172–1202, Jan. 2017.

[36] J. M. Tucker-Schwartz, T. A. Meyer, C. A. Patil, C. L. Duvall, and M. C. Skala, "*In vivo* photothermal optical coherence tomography of gold nanorod contrast agents," *Biomed. Opt. Express*, vol. 3, no. 11, pp. 2881–2895, Nov. 2012.

[37] T. Pfeiffer, M. Petermann, W. Draxinger, C. Jirauschek, and R. Huber, "Ultra low noise Fourier domain mode locked laser for high quality megahertz optical coherence tomography," *Biomed. Opt. Express*, vol. 9, no. 9, pp. 4130–4148, Sep. 2018.

[38] D. C. Adler, R. Huber, and J. G. Fujimoto, "Phase-sensitive optical coherence tomography at up to 370,000 lines per second using buffered Fourier domain mode-locked lasers," *Opt. Lett.*, vol. 32, no. 6, pp. 626–628, Mar. 2007.

[39] Y. Ling, Y. Gan, X. Yao, and C. P. Hendon, "Phase-noise analysis of swept-source optical coherence tomography systems," *Opt. Lett.*, vol. 42, no. 7, pp. 1333–1336, Apr. 2017.

[40] B. J. Vakoc, S. H. Yun, J. F. de Boer, G. J. Tearney, and B. E. Bouma, "Phase-resolved optical frequency domain imaging," *Opt Express*, vol. 13, no. 14, pp. 5483–5493, Jul. 2005.

[41] P. G. Camici and F. Crea, "Coronary microvascular dysfunction," *New England J. Med.*, vol. 356, no. 8, pp. 830–840, Feb. 2007.

[42] R. Krams *et al.*, "Effect of catheter placement on 3-D velocity profiles in curved tubes resembling the human coronary system," *Ultrasound Med. Biol.*, vol. 25, no. 5, pp. 803–810, Jun. 1999.

[43] J. J. Wentzel *et al.*, "Disturbance of 3D velocity profiles induced by an IVUS catheter: Evaluation with computational fluid dynamics," in *Proc. Comput. Cardiol.*, Sep. 1997, pp. 597–600.

[44] B. Wang *et al.*, "Gold nanorods as a contrast agent for Doppler optical coherence tomography," *PLoS ONE*, vol. 9, no. 3, Mar. 2014, Art. no. e90690.

[45] H. Assadi, V. Demidov, R. Karshafian, A. Douplik, and I. A. Vitkin, "Microvascular contrast enhancement in optical coherence tomography using microbubbles," *Proc. SPIE*, vol. 21, no. 7, Jul. 2016, Art. no. 076014.